

# Second-order Phase Transition Behavior in a Polymer above the Glass Transition Temperature

Mitsuru Ishikawa,\* Taihei Takahashi, Yu-ichiro Hayashi, Maya Akashi, Takayuki Uwada

Department of Chemistry, Faculty of Science, Josai University, 1-1 Keyaki-dai, Sakado, Saitama 350-0295, Japan

**ABSTRACT:** Glass transition was primarily considered to be not phase transition; however, it has similarity to the second-order phase transition. Recent single-molecule spectroscopy developments have prompted re-investigating glass transition at the microscopic scale, revealing that glass transition includes phenomena similar to second-order phase transition. They are characterized by microscopic collective polymer motion and discontinuous changes in temperature dependent relaxation times, later of which is similar to critical slowing down, within a temperature window that includes the polymer calorimetric glass transition temperature. Considering that collective motion and critical slowing down are accompaniments to critical phenomena, second-order phase transition behavior was identified in polymer glass transition.

## INTRODUCTION

Glass transition differs from phase transition mainly in cooling-rate dependent vitrification temperatures denoted by calorimetric glass transition temperature  $T_g$  and its analogue  $T'_g$ . [Figure 1A](#) includes liquid to crystal transition as a first-order phase transition below melting point  $T_m$ , vitrification at  $T_g$ , and cooling-rate dependent  $T_g$  and  $T'_g$ ; the difference between them can be 3–5 K on changing cooling rate by an order of magnitude.<sup>1</sup> The cooling-rate dependence repels glass transition being a phase transition. However, this figure suggests that glass transition apparently resembles second-order phase transitions. This remark defines *second-order phase transition behavior* in the present work. Glass transition is not first-order phase transition in the sense that temperature dependent  $S$  continues from liquid to glass state without discontinuous transition at  $T_g$ , although the slopes differ either side of  $T_g$ . Similarly, extrapolated  $S$  profile down to lower temperatures crosses but does not overtake crystal profile at the expected Kauzmann temperature  $T_k$  again without discontinuous transition.

We learn more second-order phase transition behavior. [Figure 1B](#) shows Arrhenius  $\eta$  traces for many glass forming materials called Angell plot.<sup>2</sup> Those for organic molecules fit the Vogel–Fulcher–Tammann (VFT) equation ([eq 1](#)), non-linear or non-Arrhenius ones between  $T_g$  and  $T_g + 50$  K,<sup>3</sup> suggesting that glass forming material viscosity  $\eta$  diverges at  $T_o$  like order parameter divergence at the critical temperature  $T_c$  in second-order phase transitions,

$$\log(\eta/\eta_\infty) = B/(T - T_o), \quad (1)$$

where  $\eta_\infty$  is the limiting viscosity at infinite temperature,  $T_o$  is the Vogel temperature, several tens K below  $T_g$ ,<sup>3</sup> and  $B$  and  $T_o$  are empirical parameters fitted from experimental observations.

The non-Arrhenius profiles in [Figure 1B](#) suggest one of critical phenomena in second order phase transitions, or collective or cooperative molecular motion.<sup>4</sup> It is assigned to  $\alpha$  process for glass forming materials. Surrounding molecules form an energy barrier that a molecule of interest must overcome to move away. This barrier increases with lowering temperature, that is, the surrounding molecules behave collectively to arrest molecule movement. Distinct spatial domains develop along with  $\alpha$  process slowdown, generating spatial heterogeneity in glass forming materials. Such heterogeneity near  $T_g$  was considered for many glass forming materials as cooperatively rearranging region (CRR),<sup>3</sup> the size of which is denoted by characteristic length  $\xi_\alpha$ , average CRR diameter. However, no  $\xi_\alpha$  divergence was found in any glass-forming materials. If

it occurs one find turbid appearance in any glass-forming materials at  $T_g$ ; this is not the case.

On the other hand, correlation length  $\xi$  divergence in collective molecular motion was found in fluid critical phenomena near  $T_c$ . These phenomena are well exemplified by the  $\text{CO}_2$  critical opalescence,<sup>4</sup> which generates a change in  $\text{CO}_2$  appearance from transparent to turbid and  $\text{CO}_2$  density fluctuations detectable by light scattering measurement, much slower than  $\text{CO}_2$  molecular motions near  $T_c$ . Turbid appearance means that  $\text{CO}_2$  molecules behave collectively in the size beyond or close to visible light wavelengths 400–700 nm.

In addition to second-order phase transition behavior from Figures 1A, 1B, and the above related consideration, we know another one. This is discontinuous change in temperature-dependent heat capacity  $C_p = T(\partial S/\partial T)_p$  evaluated by differential scanning calorimetry (DSC) to identify  $T_g$ , where a single staircase step in  $\Delta C_p$  occurs due to the discontinuous change in  $(\partial S/\partial T)_p$  between liquid and glass state. The transition interval  $\Delta T$  associated with  $\Delta C_p$  step is rather small, typically 10 K for many glass forming materials.<sup>3</sup> Generally,  $\Delta C_p$  step characterizes the second-order phase transition.<sup>4</sup>

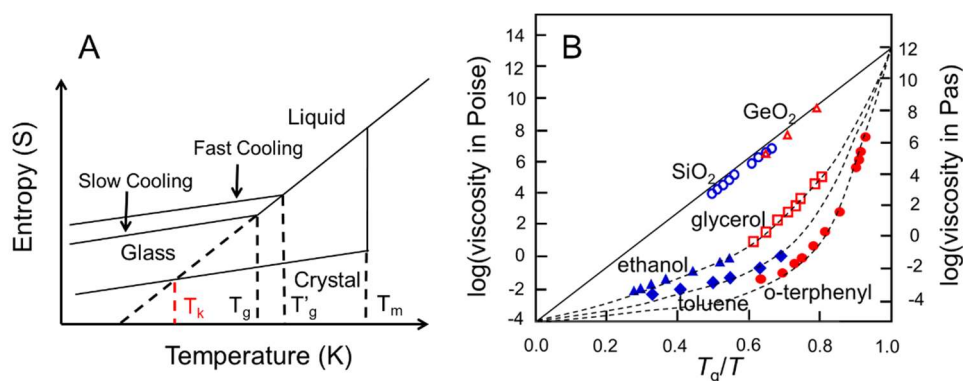


**Figure 1. Glass transition fundamentals.** (A) Temperature dependent entropy for glass forming materials including monomers and polymers, showing four important temperatures: melting point  $T_m$ , cooling-rate dependent glass transition temperatures  $T_g$  and  $T'_g$ , and Kauzmann temperature  $T_k$ ; (B) Simplified Angel plot. (A) was adapted from an article ([https://www.jps.or.jp/books/gakkaishi/2016/05/71-0570fushigi\\_09.pdf](https://www.jps.or.jp/books/gakkaishi/2016/05/71-0570fushigi_09.pdf)) by the *Physical Society of Japan*. (B) was adapted from ref 2.

Glass transition similarities in second-order phase transition motivated us to extend our early challenge by single-molecule spectroscopy (SMS) based on fluorescence and time-resolved fluorescence spectroscopy using viscosity-sensitive fluorescence probes;<sup>5–8</sup> and to quest for something unexplored. We disclosed *two major findings*, demonstrating polymer second-order phase transition behavior in a temperature window above  $T_g$ . One is substantial evidence for poly(vinyl acetate) PVAC collective motion. The other is the discontinuous change in temperature dependent PVAC average relaxation time  $\langle\tau_R\rangle$  occurring together collective motion enhancement, which looks critical slowing down<sup>9</sup> in critical phenomena in second-order phase transitions.

## RESULTS

For sample preparation and others, see *Materials and Methods* in *Supporting Information, SI*. Viscosity-sensitive Cy3 was used in single-molecule spectroscopy (SMS)<sup>6</sup> due to the fact that its fluorescence quantum efficiency  $\Phi_f$  increased with increasing solvent viscosity:  $\Phi_f = 0.042$  in fluid (297 K) and 0.94 in rigid (77 K) ethanol solution, respectively.<sup>10</sup> We selected PVAC due to its  $T_g$  above room temperature (20–25 °C) and below 40 °C suitable for the present temperature controlling setup. Figure 2A shows the SMS setup we employed in the present work, with which we collected SMS fundamental (Figures 2B–2F). All data not specified were obtained by the use of PVAC (MW 100,000).

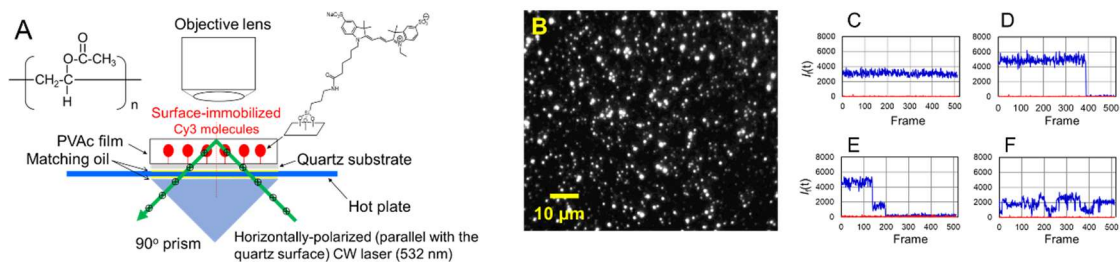


**Figure 2. Single-molecule spectroscopy (SMS) fundamentals.** (A) Experimental setup for SMS used in the present work: single Cy3 molecules covalently immobilized on a quartz surface with PVAc overlay, light microscope (shown as objective lens), quartz prism for horizontally polarized (parallel with the sample surface) evanescent illumination, and glass hot plate transparent in the visible region; (B) wide-field fluorescence image averaged over 512 frames (36 ms/frame) followed by background subtraction. Fluorescence trajectory  $I_f(t)$  for single Cy3 molecules at room temperature (24.5 °C) showing (C) no photobleaching, (D) one-step photobleaching, (E) two-step photobleaching, and (F) substantial fluctuation.

Horizontally polarized excitation (Figure 2A) allowed to collect more single-molecule fluorescence photons compared with vertically polarized excitation due to Cy3 absorption transition moment being highly oriented on a substrate surface at room temperature (23.8 °C, 1.77-fold, Figures S1A and S1B) and at an elevated temperature (56.3 °C, 1.50-fold, Figures S1C and S1D). More about the polarized excitation and circularly polarized excitation (Figures S2A and S2B) can be found in related descriptions in *Supplementary Text* in *SI*.

We applied SMS to the present glass transition-related research using surface-immobilized single molecules. To justify such application, we examined single molecule Cy3 fluorescence trajectory  $I_f(t)$  and autocorrelation functions  $C(\tau)$  evaluated from  $I_f(t)$ . Enhanced fluorescence intensities (2.16-fold, Figures S3A and S3B) with PVAc overlay and no cosine  $C(\tau)$  without PVAc overlay (Figures S4A–S4C) support single Cy3 capabilities to detect changes in PVAc environment accompanied by glass transition. More about the use of surface-immobilized probe molecules can be found in related descriptions in *Supplementary Text* in *SI*.

### Single Cy3 molecule fundamental observations

Figure 2B shows a single molecule Cy3 fluorescence image with PVAc overlay at 24.5 °C. This image was processed by averaging 512 frames (36 ms/frame), followed by background subtraction. One hundred fluorescent spots were selected to evaluate photo-bleached spots in the 512-frame acquisition: 17–23% spots were photo-bleached with PVAc overlay, whereas 35–40% spots were photo-bleached without PVAc overlay at 22–25 °C. More than 70% spots were temporally stable with PVAc overlay (Figure 2C). Single staircase photobleaching (Figure 2D) confirmed single molecule observations with rare (0.1% maximum) two-step photobleaching occurrences (Figure 2E). This means that one brighter fluorescent spot included two Cy3 molecules; a few (~5%) highly fluctuating spots also were found (Figure 2F).

### Temperature dependent single molecule fluorescence trajectories

We selected  $I_f(t)$  temporal fluctuations for 20–30 fluorescent spots that survived from photobleaching in 512-frame video acquisition in a pair of heating and cooling experiment at each temperature.

Figures 3A–3E illustrate representative  $I_f(t)$ ,  $C(\tau)$ , and power spectrum  $J(\nu)$ , Fourier transform of  $C(\tau)$ , while heating 24.5–64.9 °C. Although temperatures were elevated in a step-by-step manner: 24.5, 28.3, 29.6, 32.0, 35.6, 37.8, 41.9, 45.4, 51.9, 56.4, 60.2, and 64.9 °C at an average of 0.2 K/min (From now on, we omit “an average of” from temperature rate notations in SMS measurements, but not for DSC measurements), these figures include limited temperatures to highlight intermittent  $I_f(t)$  fluctuation and remarkable  $C(\tau)$  cosine waveforms at 41.9 and 56.4 °C

and temperature dependent specific sub-second frequencies simultaneously occurred with the once enhanced and then reduced  $J(v)$  amplitude: 0,096 at 0.109 Hz, 0.472 at 0.217 Hz, and 0.200 at 0.542 Hz, where the highest  $J(v)$  values were obtained at 29.6, 41.9, and 56.4 °C, respectively.

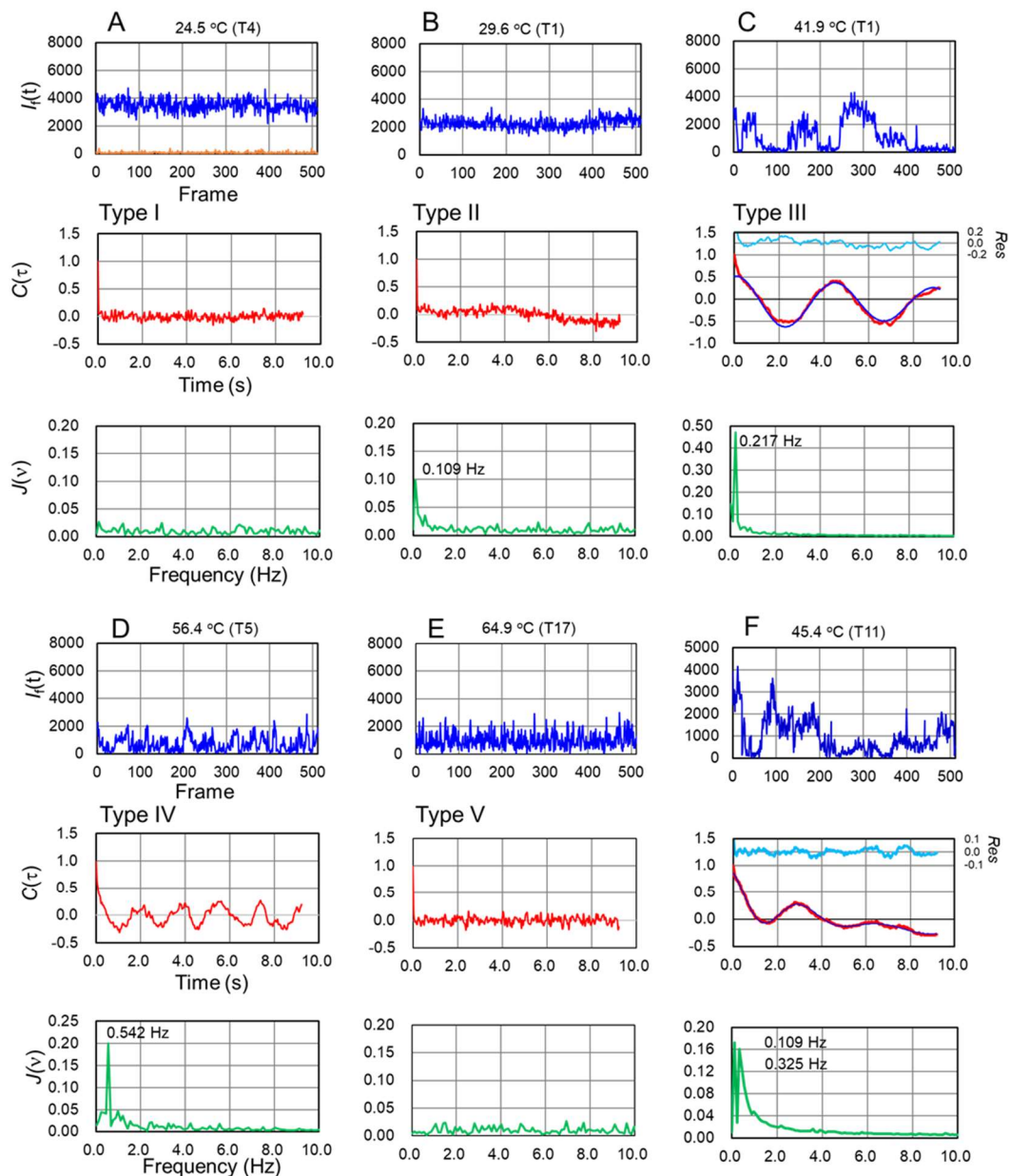


**Figure 3. Temperature dependent representative fluorescence trajectories,  $I_f(t)$ ; autocorrelation functions,  $C(\tau)$ ; and power spectra,  $J(v)$ .** They were observed from single Cy3 molecules with PVAC overlay from heating experiment (0.2 K /min) at (A) 24.5, (B) 29.6, (C) 41.9, (D) 56.4, (E) 64.9, and (F) 45.4 °C. Sets (C) and (F) include the residue (light blue trace) between experimental (red trace) and computed (blue trace) traces. Labels Type I to Type V are for  $C(\tau)$  classification. Video images generating these data were captured with horizontally polarized excitation and averaged over 512 frames (36 ms/frame) followed by background subtraction.

Cosine waveform in  $C(\tau)$ , once enhanced and then reduced  $J(v)$  amplitudes and increasing frequencies in  $J(v)$  with increasing temperature prompted us to classify  $C(\tau)$ . Figure 4A and Table S1A summarize occurrences for each  $C(\tau)$  type in Figures 3A–3E at the temperatures specified in these figures. Classification criteria for  $I_f(t)$  are as follows: Type I for stable  $I_f(t)$  and no specific

peaks in  $J(v)$ , Type II for fluctuating  $I_f(t)$  but no touching the base line with a small ( $<0.10$ ) single peak in  $J(v)$ , Type III for fluctuating  $I_f(t)$  touching base line with a prominent ( $0.20 <$ ) single peak in  $J(v)$ , and Type IV for fluctuating  $I_f(t)$  touching the base line with a prominent ( $<0.20$ ) single or multiple peaks in  $J(v)$ , and Type V for fluctuating  $I_f(t)$  touching the base line without prominent peaks ( $0.10 <$ ) in  $J(v)$ . **Type V** waveforms  $C(\tau)$  and  $J(v)$  are similar to those of Type I. For example,  $C(\tau)$ s at 56.4 °C include Type II, III, IV, and V occurrences (Figure 4A and Table S1A).

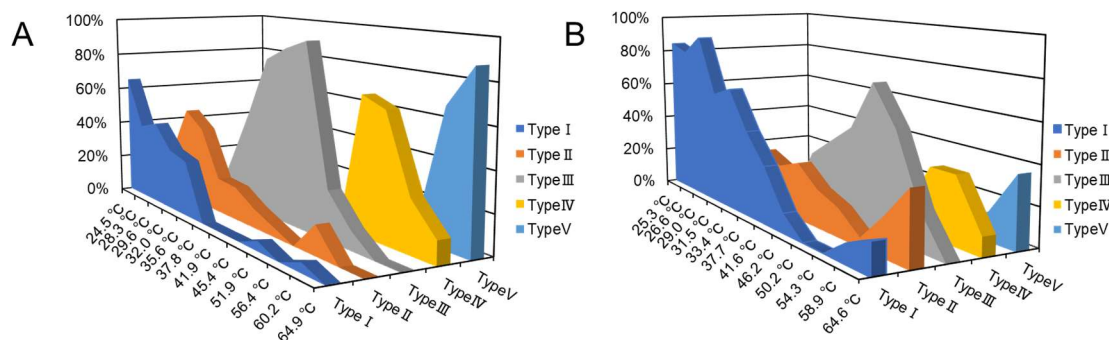


**Figure 4. Autocorrelation  $C(\tau)$  classification into six types for each observed temperature.** Type I to Type V occurrences for (A) heating 24.5–64.9 °C (0.2 K/min) and (B) cooling from 64.6–25.3 °C (0.2–0.3 K/min) are summarized. Photo-bleaching free twenty fluorescent spots from single Cy3 molecules with PVAC overlay were collected at each temperature. Video images generating these data were captured with horizontally polarized excitation and averaged over 512 frames (36 ms/frame) followed by background subtraction.

$J(v)$  amplitudes can be a measure of *purity* in cosine waveforms. We thus compared the highest  $J(v)$  0.472 at 41.9 °C with amplitude 0.930 (0.977 Hz) computed by Fourier transform of the noise-free and damping-free unitary cosine wave at 1 Hz ( $\cos 2\pi t$ ) with 36 ms bin time, showing  $> 50\%$  ( $0.472/0.930$ ) purity for  $C(\tau)$  (Figure 3C).

To avoid possible misunderstandings that all observed  $C(\tau)$  continued forever, Figure 3F shows damped  $C(\tau)$  oscillation classified into Type IV and reproduced by the sum of cosine waveforms multiplied by a single exponential decay amplitude. Damped  $C(\tau)$  oscillation was commonly observed in Type III and IV waveforms.

Figures 3A–3E show representative  $J(v)$ , with highest amplitudes from 0.096 at 29.6 °C to 0.200 at 56.4 °C and maximum overall amplitude 0.472 at 41.9 °C. To make sure that this tendency was fundamental, we evaluated  $C_{av}(\tau)$  by averaging twenty  $C(\tau)$  waveforms survived from photobleaching and computed  $J_{av}(v)$  from  $C_{av}(\tau)$  in heating experiment (Figures 5A–5L). The maximum  $J_{av}(v)$  at each temperature showed the highest peak at 41.9 °C. Figures 3C and 3F include  $C(\tau)$  damped oscillations fitted with the following functions:  $C(\tau) = C_0 \exp(-t/C_1) \{C_2 \cos(C_3 t + C_4)\} + C_5$  and  $C(\tau) = C_0 \exp(-t/C_1) \times \{C_2 \cos(C_3 t + C_4) + C_5 \cos(C_6 t + C_7) + C_8 \cos(C_9 t + C_{10}) + C_{11} \cos(C_{12} t + C_{13})\} + C_{14}$ , respectively.

In Figure 3F, we used the fitting function including *four* cosine waveforms against immediate expectation from  $J(v)$ : *two* cosine functions including two distinct frequencies 0.109 and 0.325 Hz in  $J(v)$ . This out-of-expectation fact is likely due to tailing higher than 0.325 Hz peak.

In a similar way to Figures 3A–3F, we present Figures S5A–S5F to show  $I_f(t)$ ,  $C(\tau)$ , and  $J(v)$  cooling from 64.6 to 25.3 °C at 0.2–0.3 K/min. Figure 4B and Table S1B summarize Type I to V occurrences at each temperature for cooling.

Symbols such as T1 and T17 in Figures 3A–3F, S4A–S4C, and S5A–S5F, identify fluorescence spots in the video images mainly for authors' convenience to easily trace highlighted location on the original video images.

### Relaxation time evaluation from autocorrelation functions

Representative  $C(\tau)$  showing a cosine waveform and  $J(v)$  are presented in [Figures 3C](#) and [3D](#) for heating and in [Figures S5B](#) and [S5C](#) for cooling. However,  $J(v)$  was insufficient to evaluate damped  $C(\tau)$  oscillations, such as those in [Figures 3F](#) and [S5F](#);  $J(v)$  extracted only oscillatory characteristics from  $C(\tau)$ . Thus, relaxation time  $\tau_R$  is required to extract damping behavior from  $C(\tau)$ . For this end, we used  $C_{av}(\tau)$  to cancel oscillatory characteristics, in particular frequencies higher than 0.1 Hz, from  $C(\tau)$ . We used the Kohlrausch–Williams–Watts (KWW) function  $\exp[-(t/\tau_R)^\beta]$ <sup>1, 3</sup> ( $0 < \beta < 1$ ), which has widely been used for  $\alpha$  process relaxation analysis.

We computed  $\tau_R$  from  $C_{av}(\tau)$  using

$$C_{av}(\tau) = C_o \exp\left[-(t/C_1)^{C_2}\right] + C_3 \cos(C_4 t + C_5) + C_6, \quad (2)$$

where  $C_o$ ,  $C_1 = \tau_R$ ,  $C_2 = \beta$ ,  $C_3$ ,  $C_4$ ,  $C_5$ , and  $C_6$  are fitting parameters. Note that the  $C_{av}(\tau)$  unity at  $\tau = 0$  was removed from  $C_{av}(\tau)$  to allow  $\tau_R$  computation easy; instead, the  $C_{av}(\tau)$  value at  $\tau = 0.036$  s was pasted as the value at  $\tau = 0$ . The KWW function extracts  $\tau_R$  distribution in  $C_{av}(\tau)$  through the parameter  $\beta$ . The evaluated  $C_1 = \tau_R$  is then converted into average relaxation time  $\langle\tau_R\rangle$  using

$$\langle\tau_R\rangle = \int_0^\infty e^{-(t/\tau_R)^\beta} dt = (\tau_R/\beta)\Gamma(1/\beta), \quad (3)$$

where  $\Gamma$  is the gamma function, and the area under the KWW function in [eq 3](#) denotes  $\langle\tau_R\rangle$ .<sup>11</sup> [Figures 5A–5L](#) show all the temperature dependent  $C_{av}(\tau)$ ,  $\langle\tau_R\rangle$ , and  $J_{av}(v)$ , Fourier transform of  $C_{av}(\tau)$ . The computed  $\beta$  ranged 0.45 to 1.0 and 0.36 to 1.0 for heating in [Figures 5A–5L](#) and for cooling in [Figure S6A–S6L](#), respectively. In the subsequent section, we employ  $J_{av}(v)$  to find specific temperature windows showing the maximum  $J_{av}(v)$  intensities in heating and cooling experiments.

### Temperature dependent relaxation times in a specific temperature window near $T_g$

We compared DSC measurements, temperature dependent  $J_{av}^{\max}$ , which is  $J_{av}(v)$  maxima at each temperature, and  $\langle\tau_R\rangle$  to find a temperature window in which each  $J_{av}^{\max}$  and  $\langle\tau_R\rangle$  peak was identified. [Figures 6A](#) and [6B](#) show PVAC DSC measurements for heating and cooling both at 5 K/min, respectively, in which three specific temperatures were noted:  $T_1 = 33.0$  °C (heating),  $T_2 = 43.2$  °C (cooling), and  $T_3 = 30.4$  °C (cooling). In a cooling experiment, we evaluated  $T_g = 36.5$  °C (309.5 K) from the midpoint of the gap between extrapolated glass and melt lines. The reason for  $T_g$  evaluation by cooling is based on a series of heating, cooling, and again heating DSC measurements ([Figures S7A–S7C](#)) with three temperature rates, 5, 10, 20 K/min. Only cooling experiment presented consistent results showing 36.0–36.3 °C as  $T_g$  from the midpoint evaluation irrespective of the different temperature rates, confirming that cooling from melt erases the inhomogeneous glass structure memory.

[Figure 6A](#) shows another temperature zone under the dotted line above  $T_1 = 33.0$  °C characterized by enthalpy overshoot,<sup>12</sup> which is an endothermic process intrinsic to heating DSC. This overshoot always occurred in our observations ([Figures S7A–S7C](#)). In contrast, no enthalpy overshoots were observed for cooling experiments ([Figure 6B](#) and [Figures S7A–S7C](#)). Note that the heating DSC trace in [Figure 6A](#) total differs from the heating traces in [Figures S7A–S7C](#), which shows enthalpy overshoot much larger than that in [Figure 6A](#). The difference reflects difficulties in getting reproducible heating DSC traces.

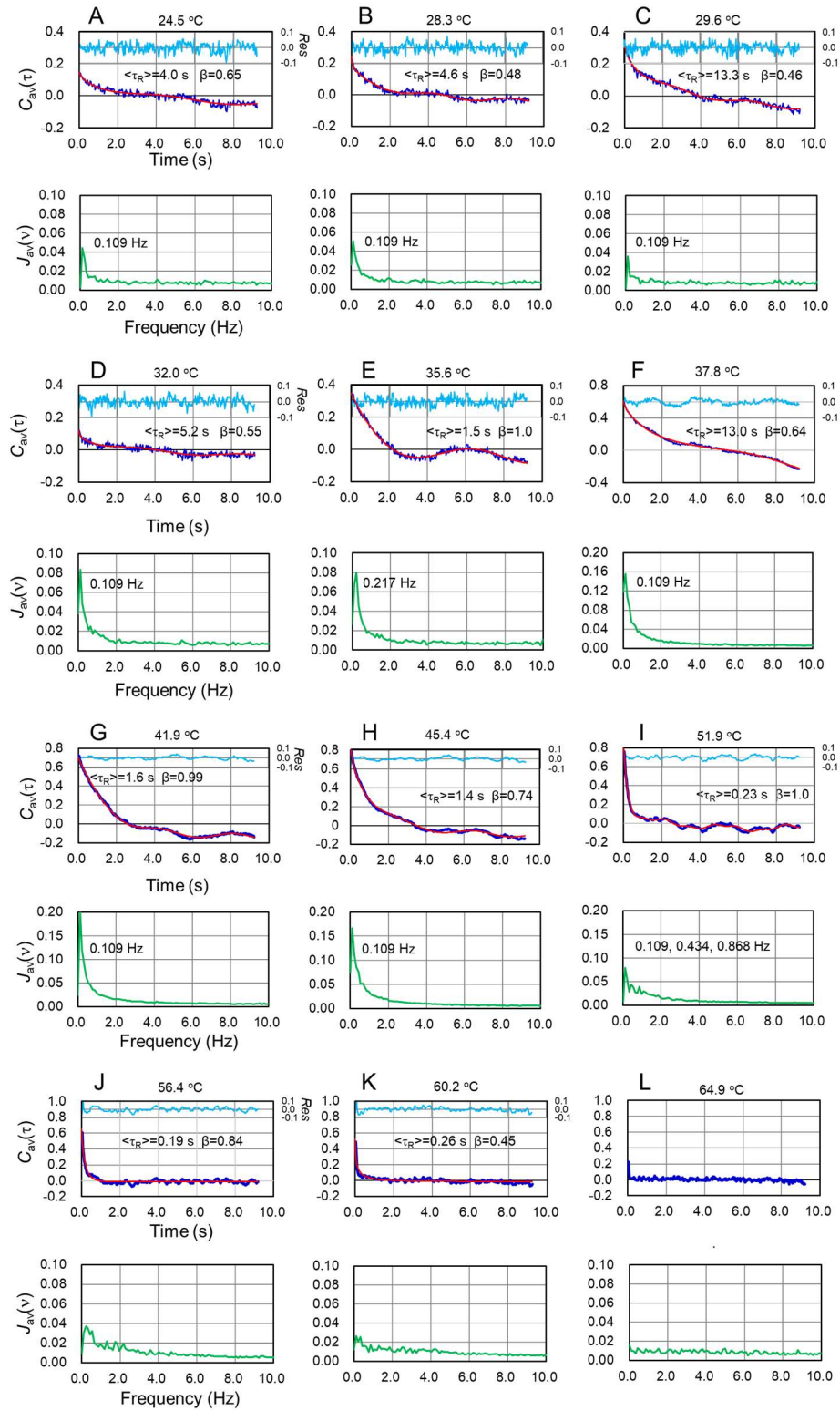


**Figure 5. Average autocorrelation functions,  $C_{av}(\tau)$  and power spectra,  $J_{av}(v)$ .** They were observed for heating (0.2 K/min) from single Cy3 molecules with PVAC overlay and computed from twenty single Cy3 molecules free from photobleaching at (A) 24.5, (B) 28.3, (C) 29.6, (D) 32.0, (E) 35.6, (F) 37.8, (G) 41.9, (H) 45.4, (I) 51.9, (J) 56.4, (K) 60.2, and (L) 64.9 °C. In (L),  $\langle \tau_R \rangle$  evaluation was halted due to inability to identify decay in  $C_{av}(\tau)$ . Each  $C_{av}(\tau)$  trace except for (L) was fitted with eq 2 and includes calculated trace (red) and parameters  $\langle \tau_R \rangle$  and  $\beta$ , together with residue between experimental and calculated traces (light blue).

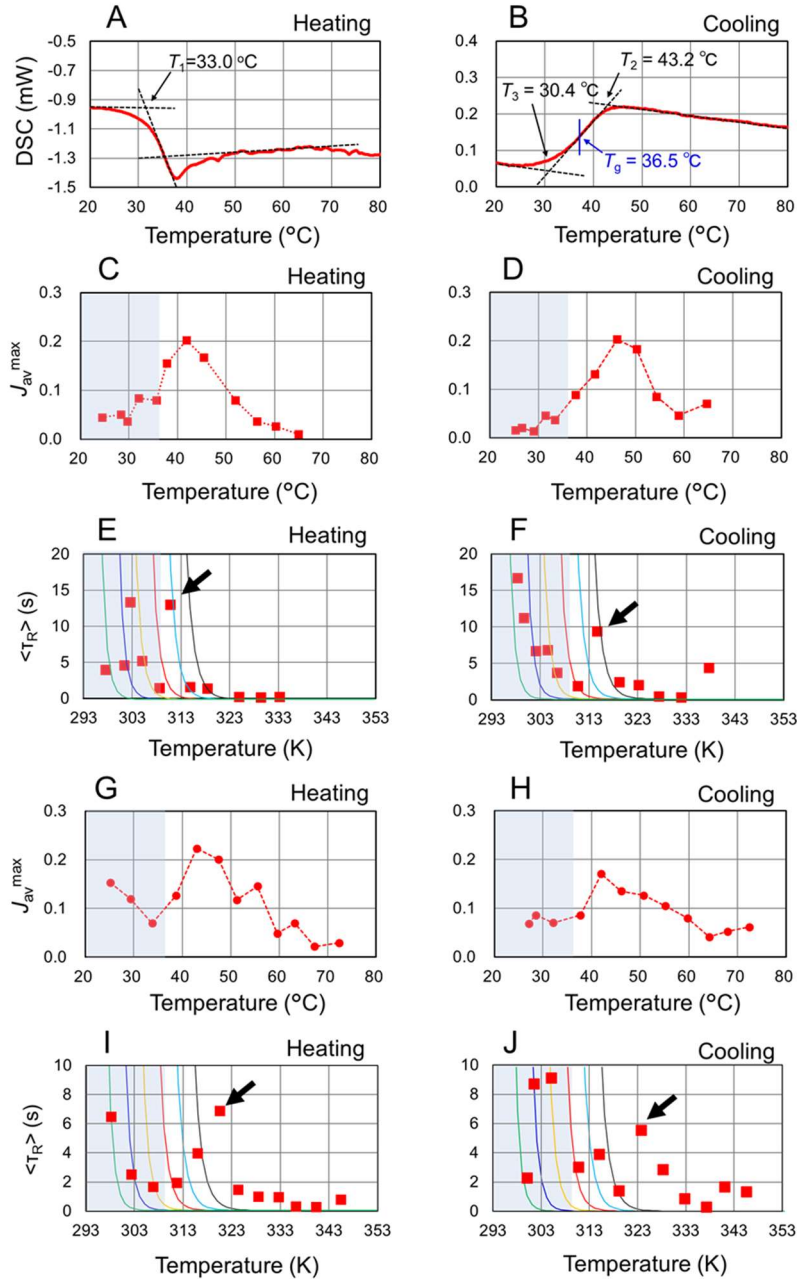


**Figure 6. DSC measurements; temperature dependent average power spectra maxima,  $J_{av}^{max}$ ; and temperature dependent average relaxation time,  $\langle \tau_R \rangle$  superposed with VFT lines:** DSC traces for (A) heating and (B) cooling (both 5.0 K/min);  $J_{av}^{max}$  for (C) heating (0.2 K/min) and (D) cooling (0.2–0.3 K/min);  $\langle \tau_R \rangle$  for (E) heating and (F) cooling (0.2–0.3 K/min). VFT lines ( $B = 460, 510, 560, 610, 660,$  and  $710$  K in green, blue, orange, red, light blue, and gray, respectively, computed from eq 4 using each  $B$  value) are superposed on the  $\langle \tau_R \rangle$  plot. From another pair of heating and cooling (both 1 K/min) experiments using PVAC (MW 500,000), we obtained (G), (H), (I) and (J). The VFT lines for  $B = 610, 660,$  and  $710$  K were experimentally identified.<sup>13</sup> Arrows in (C), (D), (I), (J) specify discontinuously enhanced  $\langle \tau_R \rangle$  peaks. The temperature zones in a shaded blue indicate those below  $T_g = 36.5^\circ\text{C}$ . The standard deviation  $\pm\sigma$  of each data point in (E) was within the marker size except for 9.96 s at 302.6 K. In (F), 94.3 s, 12.1 s, 7.0 s, 3.4 s, 2.1 s, 6.5 s, and 3.6 s are beyond the marker size at 298.3 K, 299.6 K, 302.0 K, 304.5 K, 306.4 K, 314.6 K, and 337.6 K, respectively. In (I), all  $\pm\sigma$  was within the marker size. In (J), 1.31 s, 8.18 s, and 1.68 s are beyond the marker size at 301.5 K, 305.1 K, and 332.7 K, respectively.

A set of temperature dependent  $J_{av}^{\max}$  and  $\langle\tau_R\rangle$  was acquired from the same SMS movie at each temperature. Thus, Figures 6C and 6E were assembled from the same sample; alike Figures 6D and 6F, Figures 6G and 6I, and Figures 6H and 6J. Heating and cooling experiments were carried out using separate samples from the same preparation lot.

Two  $J_{av}^{\max}$  peaks at 41.9 (Figure 6C, heating) and 46.2 °C (Figure 6D, cooling) are separated by  $\approx 4$  K. It is likely due to hysteresis between heating and cooling. However, another pair of heating and cooling experiments using PVAC (MW 500,000), Figure 6G (heating at 1 K/min) and Figure 6H (cooling at 1 K/min), exhibited no substantial hysteresis. Such small hysteresis varied from experiment to experiment in an uncontrollable manner, independent of MW 100,000 or 500,000 and heating and cooling rate (1 K/min or slower); the different hysteresis observations cannot be ascribed to the MW and temperature rate difference. Thus, importance is in the fact that heating and cooling experiments identified  $J_{av}^{\max}$  reaching the top between  $T_g$  and nearly  $T_g + 10$  K.

In the comparison between temperature dependent  $\langle\tau_R\rangle$  in a heating and cooling pair in Figures 6E and 6F and another pair in Figures 6I and 6J using PVAC (MW 500,000), we experienced the comparison similar to that between heating  $J_{av}^{\max}$  and cooling  $J_{av}^{\max}$  peaks. Again, importance is in the fact that  $\langle\tau_R\rangle$  reached the top pointed by arrows between  $T_g$  and nearly  $T_g + 10$  K independent of MW. This mention is reasonable considering that  $T_g$  of PVAC (MW 500,000) was almost equal to that of PVAC (MW 100,000) (Figures S8A–S8C).

To compare the temperature dependent  $\langle\tau_R\rangle$  with temperature dependent relaxation times evaluated by dielectric loss spectroscopy, we computed VFT lines using another VFT equation

$$\log(\omega_\infty/\omega_{\max}) = B/(T - T_o), \quad (4)$$

where  $\omega_\infty$  is the limiting angular velocity at infinite temperature, using  $B = 660 \pm 50 \text{ K}^{12}$  in addition to other three  $B$  values we selected, and then converted  $\omega_{\max} = 2\pi\nu$  into  $\langle\tau_R\rangle$  from  $1/\nu = \langle\tau_R\rangle$ . The computed VFT lines are superposed on Figures 6E, 6F, 6I, and 6J, showing that enhanced  $\langle\tau_R\rangle$  substantially followed the VFT lines.

## DISCUSSION

First of all, we remind us of glass transition fundamentals from dielectric spectroscopy to reveal significance and to find technical limitations in the present work, and then provide supplementary views about each experimental observation and substantial consideration to observations related to the two major findings. After that we develop arguments to help understand the two major findings.

Cooling glass forming liquids below  $T_m$  and close to the crossover temperature  $T_{\text{cross}} \approx 1.2T_g$ , consistent with mode-coupling theory (MCT) expectation,<sup>1,14</sup> splits a single dielectric-loss peak into faster and slower ones.<sup>1</sup> Dynamics characterized by the slower frequency is  $\alpha$  process and that characterized by the faster frequency is  $\beta$  process. Alpha process exhibits non-Arrhenius behavior and almost disappears below  $T_g$ , whereas  $\beta$  process continues Arrhenius behavior below  $T_g$ . The  $\tau_R$  for  $\alpha$  process, typically 0.1–1.0 s, at  $T_g + 10$ –20 K, is much slower ( $> 10^7$ -fold) than that for  $\beta$  process at  $T_g$ .<sup>1,3</sup> Our SMS technique lacked temporal resolution to detect  $\beta$  process; we only considered  $\alpha$  process assigned to polymer main chain segment Brownian motion (micro-Brownian motion) characterized by cooperative nature. The size of cooperative regions, or CRR, near  $T_g$  giving heterogeneity in many glass forming materials was estimated at 1–5 nm.<sup>1, 15–17</sup>

### Four-fold supplementary views about each experimental observation

First, fluorescence intensity varied from spot to spot (Figure 2B). This was partly due to excitation light polarization and photo-bleached spots in the image acquisition, but mainly due to highly heterogeneous polymer structures probed by SMS. Second, we should follow the identical single Cy3 molecules from start to finish in all SMS measurement; however, photobleaching prohibited such ideal measurement. This is a fundamental SMS limitation. Third, we provided consideration to ascertain the validity of single Cy3 molecules sensing PVAC environment

(Figures S3A and S3B; Figures S4A–S4C), and then discussed glass transition at interfaces and sub-second  $J(\nu)$  frequency origins in Figures 3B–3D, 3F, S5A–S5D, and S5F in *Supplementary Text* in SI. A proposed scheme to explain intermittent  $I_f(t)$  fluctuation (Figures 3C–3F) as well as Cy3 photophysics behind  $I_f(t)$  fluctuation is summarized in Figures S9A–S9D in *Supplementary Text* in SI. Last, we used the product of one single exponential function and one cosine function or cosine function summation to treat  $I_f(t)$  as a single damped oscillator in a conventional manner (Figures 3F and S5F). However, the sum of the KWW and a cosine function in eq 2 was used in Figures 5A–5L and Figures S6A–S6L simply because the product did not generate acceptable fitting between  $C_{av}(\tau)$  and the calculated one, such as no convergence fitting from the start, negative  $C_0$ , and  $C_2$  larger than 1.0 in eq 2. From eq 2 we extracted only the relaxation term and evaluated  $\langle \tau_R \rangle$  through eq 3. This procedure follows fluctuation-dispersion theorem.

### Three-fold substantial consideration to observations related to the two major findings

(i) Temperature dependent  $C(\tau)$  evaluated from  $I_f(t)$  (Figures 3A–3F for heating and Figures S5A–S5F for cooling) included remarkable  $C(\tau)$  cosine waveforms, hence providing evidence for collective PVAC motion above  $T_g$ . This is *the first major finding*, PVAC collective motion, which is deduced from the generalized Langevin equation (GLE)<sup>18</sup> under the approximation leading to the understanding that PVAC environment coherently and persistently influences viscosity sensitive single Cy3 molecule fluorescence.

(ii) Our consideration to the observations in Figures 6A–6J depends on the assumption that  $T_g$  at interfaces between PVAC thin films and quartz surfaces (Figure 2A) is close to  $T_g$  evaluated by DSC. One finds more about this assumption in *Supplementary Text* in SI.

(iii) From  $\langle \tau_R \rangle$  evaluation, we found *the second major finding*, discontinuous  $\langle \tau_R \rangle$  change in a specific temperature window in which PVAC collective motion was activated. From the observations in Figures 6C–6J, what we can mention is the fact that  $\langle \tau_R \rangle$  peaks occurred in the same temperature window where enhanced  $J_{av}^{max}$  were observed. Enhanced  $\langle \tau_R \rangle$  with decreasing temperature below  $T_g = 36.5$  °C is reasonable due to increased viscosity at lower temperatures and Cy 3 viscosity-sensitive nature. From the VFT line superposition (Figures 6E, 6F, 6I, and 6J), the  $\langle \tau_R \rangle$  peaks are out of conventional expectation.

### Derivation of the $C(\tau)$ cosine waveform from generalized Langevin equation

The normalized autocorrelation function  $C(\tau)$  is defined as

$$C(\tau) = R(\tau)/R(0), \quad (5)$$

where  $R(\tau)$  is the autocorrelation function and  $R(0)$  is a normalizing factor. Before evaluating  $C(\tau)$  we computed  $R(\tau)$  from  $I_f(t)$

$$R(\tau) = \frac{1}{N} \sum_i^N I_f^o(i) I_f^o(i+\tau) \equiv \langle I_f^o(i) I_f^o(i+\tau) \rangle, \quad (6)$$

where  $I_f^o(i) = I_f(i) - \bar{I}_f$ ;  $\bar{I}_f$  is average  $I_f(t)$  over 512 frames,  $N = 256$  is the number of data points (half the number of the total frames) with step size or bin time  $\Delta t = 36$  ms,  $i$  and  $\tau$  denote each data point.

We summarize cosine autocorrelation function derivation<sup>19</sup> from the GLE

$$\frac{dA(t)}{dt} = i\omega_o A(t) - \int_0^t \varphi(t-t') A(t') dt' + f(t), \quad (7)$$

where  $A(t)$  is a dynamical variable (generally a vector),  $\omega_o$  is a formal angular frequency (generally a matrix with zero diagonal elements),  $f(t)$  is a randomly fluctuating external force, and  $\varphi(t-t')$  is a memory function combining  $A(t)$  at  $t'$  (past) and  $t$  (present) given by

$$\varphi(t-t') = \frac{\langle f(t) f(t') \rangle}{\langle f(0) f(0) \rangle}, \quad (8)$$

Equation 8 is an essential result from GLE formulation,<sup>18</sup> signifying that the memory function is explicitly combined with normalized external force time correlation function. This equation is also a kind of fluctuation dispersion theorem. For the present derivation,  $A(t)$  is a scalar variable equivalent to  $I_f(t)$ ; hence  $\omega_0 = 0$  because it is a  $[1 \times 1]$  dimensional matrix with zero diagonal.

GLE is applicable to Brownian motion analyses, and its use here is quite reasonable considering that polymer dynamics are modeled as polymer segment micro-Brownian motion. After several derivation steps from eq 7 (the skipped derivations are provided in *Supplementary Text* in *SI*),

$$\frac{d\Phi(t)}{dt} = -\omega^2 \int_0^t \varphi(t-t')\Phi(t') dt', \quad (9)$$

where  $\omega^2$  is constant and  $\Phi(t)$  is a normalized autocorrelation function equivalent to  $C(\tau)$ ,

$$\Phi(t) = \frac{\langle A(t)A(0) \rangle}{\langle A(0)A(0) \rangle}, \quad (10)$$

where  $\langle A(t)A(0) \rangle$  is an autocorrelation function of  $A(t)$ . Substituting  $\varphi(t-t') = 1$  into eq 9, that is, no memory function extinction approximation,<sup>19</sup> gives

$$\frac{d\Phi(t)}{dt} = -\omega^2 \int_0^t \Phi(t') dt' \quad (11)$$

and hence

$$\Phi(t) = \cos \omega t \quad (12)$$

because  $\Phi(0) = 1$  from the normalized autocorrelation function definition. Thus, we have a cosine autocorrelation function with no memory function extinction approximation. This provides the rationale for cosine  $C(\tau)$  waveforms (Figures 3C and S5C) and can be explained as follows.

No memory function extinction means  $\langle f(t)f(t') \rangle \approx \varphi(t-t') = \text{constant}$ , that is,  $f(t)$  shows how PVAC collective motion coherently and persistently affects single Cy3 molecules as Brownian particles. On the other hand, instantaneous  $\varphi(t-t')$  disappearance approximation provides a single exponential decay  $C(\tau)$ . Damped oscillation (Figures 3F and S5F) as an intermediate waveform between cosine and single exponential decay was dominantly observed. Figures S10A and S10B compare the two approximations for GLE in *SI*.

### Discontinuous change in temperature-dependent relaxation time above $T_g$

Temperature dependent  $J_{av}^{\max}$  (Figures 6C, 6D, 6G, and 6H) disclosed a temperature window between  $T_g = 36.5$  °C (309.5 K) and  $T_g + 10$ – $20$  K. Temperature dependent  $\langle \tau_R \rangle$  (Figures 6E, 6F, 6I, and 6J) pinpointed specific temperatures within the temperature window, showing the second major finding. These temperatures are considerably less than  $T_{\text{cross}} \approx 1.2T_g = 371.4$  K (98.4 °C). Thus, the temperature window characterized by highly fluctuating collective PVAC motions embodied by the  $C(\tau)$  cosine waveform appears outside MCT expectation but involves cooperative  $\alpha$  process active temperature zone.

We examine the significance of  $\langle \tau_R \rangle$  discontinuous change generating peaks (Figures 6E, 6F, 6I, and 6J). These temperatures fall within the temperature window where  $J_{av}^{\max}$  was enhanced (Figures 6C, 6D, 6G, and 6H). Higher  $J_{av}^{\max}$  amplitude was associated with activated  $C_{av}(\tau)$  cosine or oscillatory characteristics (Figures 5A–5K and S6A–S6L). We thus consider the temperatures giving  $\langle \tau_R \rangle$  peaks to be  $T_c$  (heating) and  $T_c'$  (cooling) from the following discussion.

Perfect cosine  $C(\tau)$  without damping shows infinite  $\tau_R$ . In practice,  $\langle \tau_R \rangle$  exhibited limited-height peaks within the temperature window between  $T_g = 36.5$  °C (309.5 K) and  $T_g + 10$ – $20$  K in which  $C_{av}(\tau)$  cosine characteristics, collective PVAC motion, were activated. Thus, the  $\langle \tau_R \rangle$  peaks look equivalent to order parameter discontinuity in the second-order phase transition or critical phenomena<sup>4</sup> because of their simultaneous occurrences with activated collective PVAC motion. Thus,  $\langle \tau_R \rangle$  discontinuity associated with PVAC collective motion reminds us of critical slowing down, which is a critical phenomenon in the second-order phase transition.

Critical slowing down provides divergent  $\tau_R$  near  $T_c$ <sup>9</sup>

$$\tau_R \propto \frac{1}{(T - T_c)^\gamma}, \quad (13)$$

where  $\gamma$  is a critical-point exponent. A moving particle on a potential energy curve models critical slowing down as follows.<sup>20</sup> Consider a particle on the Gibbs potential designated by pressure  $p$  and  $T$  having two minima. Below  $T_c$  changing  $p$  or  $T$  allows the particle to move from one higher minimum to the lower one, generating the first-order phase transition. At  $T_c$  the second-order phase transition occurs; two potential minima are merged into one, and the one-minimum potential is flattened, which is formulated in Landau theory. Thus, the particle moves slowly and widely on the flattened potential surface. The slowly moving particle models critical slowing down.

Equation 13 is equivalent to that of temperature dependent isothermal magnetic susceptibility  $\chi_T$  in magnets and isothermal compressibility  $\kappa_T$  in fluids. The  $\gamma$  value is unity from the mean-field theory and Landau theory, but experimentally 1.2–1.4.<sup>4, 9, 20</sup> We restrict serious  $\gamma$  value evaluation from Figures 6E, 6F, 6I, and 6J in the present work; however,  $\gamma = 0.5$  was unrealistic but  $\gamma = 1$  was possible, and discrimination between  $\gamma = 1$  and  $\gamma = 1.5$  was hard to do in the limited number of data points in the tentative evaluation from these figures. The present work mission does not involve rigorous  $\gamma$  evaluation but SMS application to glass transition issue elucidation. Experimental challenges to estimate more rigorously  $\gamma$  values are now underway. Thus, the second-order phase transition behavior was observed not only in cosine  $C(\tau)$  but also in temperature dependent discontinuous  $\langle\tau_R\rangle$  changes.

Discontinuous change in  $\langle\tau_R\rangle$  was reproduced in several pairs of heating and cooling SMS experiments; however, the temperatures showing the peak  $\langle\tau_R\rangle$  were different from heating to cooling and experiment to experiment. The varied  $\langle\tau_R\rangle$  peak occurrences can be rationalized as follows. In the present SMS, we employed surface immobilized sub-nanometer size Cy3 probes allowing spatially resolved measurement in the nanometer region. We thus assume that not all the probed sites in PVAC present second-order phase transition behavior. For example,  $C(\tau)$  in Type III did not exclusively occur within  $T_g = 36.5^\circ\text{C}$  (309.5 K)– $T_g + 10$ – $20$  K window especially at  $T_g + 10$  K (Figures 4A and 4B; Tables S1A and S1B). Note that  $\langle\tau_R\rangle$  was evaluated from  $C_{av}(\tau)$  averaged over every  $C(\tau)$  including Type I to Type V at each temperature, likely generating varied  $\langle\tau_R\rangle$  peaks.

An early model,<sup>21</sup> in which super cooled liquids include dispersed micro-crystals, inspires the idea of specific sites showing second-order phase transition behavior in PVAC. This model predicts the widely known empirical relationship  $T_g/T_m \approx 2/3$ , making this model reliable. For this reason, our assumption considering the sites specific to second-order phase transition behavior in PVAC seems to be far from groundless. The idea of super cooled liquids including dispersed micro-crystals have developed into super cooled liquids as mosaic states, which are modeled in random first-order transition (RFOT) theory.<sup>22</sup> Single Cy3 molecules might probe such mosaic states in PVAC and disclosed PVAC heterogeneity showing second-order phase transition behavior. We have no idea at this moment to combine “first-order” in RFOT and “second-order” in the present observations. We have started consideration to the present work from thermodynamic and dynamic phenomenology showing similarities in second-order phase transition symbolized by Figures 1A and 1B, respectively. In this context, “random second-order transition theory” can be proposed only by superficial word meanings.

## CONCLUSIONS

We identified two sets evidence for second-order phase transition behavior in PVAC glass transition: highly active PVAC collective motions from  $C(\tau)$  cosine waveforms above  $T_g$  and discontinuous transition in temperature dependent  $\langle\tau_R\rangle$ . These findings appeared beyond the known theoretical framework for glass transition and related phenomena, such as MCT. The two

major findings provided evidence suggesting that glass transition includes second-order phase transition behavior above  $T_g$ . The present major findings have been disclosed by single molecule probes making it possible to directly detect polymer segment micro-Brownian motion.

Second-order phase transition behavior in glass transition has been suggested in temperature dependent  $S$ ,  $C_p$ , and  $\eta$  as noted in *Introduction*. These parameters temperature dependence is solid experimental facts. However, such knowledge has lacked straightforward evidence for critical phenomena in glass transition mainly due to experimental limitations.

The major findings arose from SMS, which is an unconventional method for glass transition investigation in contrast to the more widely used DSC, dielectric and mechanical spectroscopy, and others. However, SMS in the present our status has one inability and one technical limitation in return for the uniqueness demonstrated in the present work. The inability is that no direct  $\xi_\alpha$  evaluation but no critical opalescence observation from PVAC, suggesting  $\xi_\alpha < 100\text{--}200$  nm. The limitation is photobleaching in Cy3, or most fluorescent dyes. This issue prevents repeated video imaging, which limits the number of  $\langle\tau_R\rangle$  data points.

#### ASSOCIATED CONTENT

##### Corresponding Author

\*E-mail: mi195526@josai.ac.jp

##### ORCID

Mitsuru Ishikawa: 0000-0001-9438-2270

Takayuki Uwada: 0000-0002-4272-7964

**Funding:** This work was supported by graduate and undergraduate student research budgets in Department of Chemistry, Josai University; no other funding was involved such as Kaken-hi (MEXT) in the present work. **Author contributions:** M. I. planned this work, supervised three students, T. T., Y. H., and M.A. and wrote the manuscript. T. T. joined this work for three years as an undergraduate and a graduate student, contributing to experiment and data analysis. Y. H. and M. A. also joined this work for one year each as undergraduate students and contributed to part of experiment and data analysis. T. U. also supervised T. T. to complete his master's thesis involving this work. **Competing interests:** All the authors have no competing interests. **Data and material availability:** All data necessary for evaluating the conclusions in the present work are included in the manuscript and *SI*.

#### ACKNOWLEDGMENTS

M. I. thanks Prof. Vasudevan Pillai Biju, Research Institute for Electronic Science, Hokkaido University, for his kind advice and support for sample preparation, and also for permitting the use of Figures S9A–S9C, the original of which was prepared by himself. Also, Prof. Yoshihiro Tokudome, Department of Pharmaceutical Sciences, Josai University, is appreciated by M. I. for his technical advice for DSC equipment operation in 2019.

## REFERENCES

1. P. G. Debenedetti, F. H. Stillinger, Supercooled liquids and the glass transition. *Nature* **410**, 259–267 (2001).
2. C. A. Angell, K. L. Ngai, G. B. McKenna, P. F. McMillan, S. W. Martin, Relaxation in glassforming liquids and amorphous solids. *J. Appl. Phys.* **88**, 3113–3157 (2000).
3. E. Donth, “1. Introduction” and “2.1. The classical picture. No serious problems” in *The Glass Transition, Relaxation Dynamics in Liquid and Disordered Materials*, (Springer 2001), pp 1–66.
4. H. E. Stanley, “What are the critical phenomena? A survey of some basic results” in *Introduction to phase transitions and critical phenomena*, (Oxford 1971), pp. 1–21.
5. M. Ishikawa, J. Y. Ye, Y. Maruyama, H. Nakatsuka, Triphenylmethane dyes revealing heterogeneity of their nanoenvironment: femtosecond, picosecond, and single-molecule studies. *J. Phys. Chem. A* **103**, 4319–4331 (1999).
6. V. P. Biju, J. Y. Ye, M. Ishikawa, Spatial heterogeneity in a polymer thin film probed by single molecules. *J. Phys. Chem. B* **107**, 10729–10735 (2003).
7. J. Y. Ye, T. Hattori, H. Inouye, H. Ueta, H. Nakatsuka, Y. Maruyama, M. Ishikawa, Glass transition of associated solvents studied by fluorescence measurement of doped chromophores. *Phys. Rev. B* **53**, 8349–8353 (1996).
8. J. Y. Ye, T. Hattori, H. Nakatsuka, Y. Maruyama, M. Ishikawa, Microscopic dynamics of the glass transition investigated by time-resolved fluorescence measurements of doped chromophores. *Phys. Rev. B* **56**, 5286–5295 (1997).
9. H. Nishimori, G. Ortiz, “2.11 Dynamic critical phenomena” in “Elements of phase transitions and critical phenomena”, (Oxford, 2011), pp 46–51.
10. K. Chibisov, G. V. Zakharova, H. Görner, Yu. A. Sogulyaev, I. L. Mushkalo, A. I. Tolmachev, Photorelaxation processes in covalently linked indocarbocyanine and thiocarbocyanine dyes. *J. Phys. Chem.* **99**, 886–893 (1995).
11. T. Oba, M. Vach, Relaxation in thin films mapped across the film thickness by astigmatic single-molecule imaging. *ACS Macro Lett.* **1**, 784–788 (2012).
12. McKenna, G. B.; Simon, S. L. 50<sup>th</sup> Anniversary perspective: challenges in the dynamics and kinetics of glass-forming polymers. *Macromolecules* **50**, 6333–6361 (2017).
13. M. Beiner, J. Korus, H. Lockwenz, K. Schröter, E. Donth, Heat capacity spectroscopy compared to other linear response methods at dynamic glass transition in poly(vinyl acetate). *Macromolecules* **29**, 5183–5189 (1996).
14. H. Sillescu, Heterogeneity at the glass transition: a review. *J. Non-Cryst. Solids* **243**, 81–108 (1999).
15. M. D. Ediger, Spatially heterogeneous dynamics in supercooled liquids. *Annu. Rev. Phys. Chem.* **51**, 99–128 (2000).
16. U. Tracht, M. Wilhelm, A. Heuer, H. Feng, K. Schmidt-Rohr, H. W. Spiess, Length scale of dynamic heterogeneities at the glass transition determined by multidimensional nuclear magnetic resonance. *Phys. Rev. Lett.* **81**, 2727–2730 (1998).
17. E. Hempel, G. Hempel, A. Hensel, C. Schick, E. Donth, Characteristic length of dynamic glass transition near  $T_g$  for a wide assortment of glass-forming substances. *J. Phys. Chem. B* **104**, 2460–2466 (2000).
18. H. Mori, Transport, collective motion, and Brownian motion. *Prog. Theor. Phys.* **33**, 423–455 (1965).
19. H. Shimizu, “Kanwa-gensyo no kiso (Fundamentals in relaxation phenomena)” in *Kanwa-gensyo no kagaku (Relaxation phenomena in chemistry)*, Eds. K. Higashi, S. Nagakura (Iwanami, 1973), pp 5–73 (in Japanese).
20. H. B. Callen, “Critical phenomena” in “Thermodynamics and introduction to thermostatistics” 2<sup>nd</sup> Ed. (Wiley, 1985), pp 255–275.

21. W. Kauzmann, The nature of the glassy state and the behavior of liquids at low temperatures. *Chem. Rev.* **43**, 219–256 (1948).
22. T. R. Kirkpatrick, D. Thirumalai, “Random first-order phase transition theory of the structural glass transition” in “Structural glasses and supercooled liquids”, Eds. P. G. Wolynes, V. Lubchenko (Wiley, 2012), pp 223–236.
23. F. Köhn, J. Hofkens, R. Gronheid, M. Van der Auweraer, F. C. De Schryver, Parameters influencing the on- and off-times in the fluorescence intensity traces of single cyanine dye molecules. *J. Phys. Chem. A* **106**, 4808–4814 (2002).
24. H. Mortazavian, C. J. Fennell, F. D. Blum, Structure of the interfacial region in adsorbed poly(vinyl acetate) on silica. *Macromolecules* **49**, 298–307 (2016).
25. K. Jia, Y. Wan, A. Xia, S. Li, F. Gong, G. Yang, Characterization of photoinduced isomerization and intersystem crossing of the cyanine dye Cy3. *J. Phys. Chem. A* **111**, 1593–1597 (2007).
26. N. J. Turro, “Photophysical radiationless transitions” in *Modern Molecular Photochemistry* (Addison–Wesley, ed. 2, 1978), pp 153–198.
27. S. Yu. Grebenkin, B. V. Bol’shakov, Cage effects upon light irradiation on azo compounds: *cis* → *trans* isomerization in polymethyl methacrylate. *J. Photochem. Photobiol., A* **122**, 205–209 (1999).